Comparison of near-forward light scattering on oceanic turbulence and particles

Darek J. Bogucki, J. Andrzej Domaradzki, Dariusz Stramski, and J. Ronald Zaneveld

We examine and compare near-forward light scattering that is caused by turbulence and typical particulate assemblages in the ocean. The near-forward scattering by particles was calculated using Mie theory for homogeneous spheres and particle size distributions representative of natural assemblages in the ocean. Direct numerical simulations of a passive scalar with Prandtl number 7 mixed by homogeneous turbulence were used to represent temperature fluctuations and resulting inhomogeneities in the refractive index of water. Light scattering on the simulated turbulent flow was calculated using the geometrical-optics approximation. We found that the smallest temperature scales contribute the most to scattering, and that scattering on turbulence typically dominates over scattering on particles for small angles as large as 0.1°. The scattering angle deviation that is due to turbulence for a light beam propagating over a 0.25-m path length in the oceanic water can be as large as 0.1°. In addition, we carried out a preliminary laboratory experiment that illustrates the differences in the near-forward scattering on refractive-index inhomogeneities and particles. © 1998 Optical Society of America

OCIS codes: 010.7060, 290.4020, 080.2710.

1. Introduction

The passage of an electromagnetic beam through a turbulent medium results in a change of light velocity which in turn causes distortion in intensity and phase of the beam. We refer to any process through which the path of an individual photon is changed as scattering. In realistic seawater the light beam scattered into near-forward directions originates either from interaction with refractive-index inhomogeneities of water or particles (molecular near-forward scattering is usually negligible). Oceanic measurements of small-angle scattering[1] show that the volume-scattering function exhibits a sharp peak that is orders of magnitude greater than that obtained from either the laboratory measurements of Spinrad *et al*.[2] or the Mie-type calculations for nonturbulent conditions.[3] This effect, i.e., peaking of the volume-scattering function at small angles, has been attributed to scattering by turbulence-induced inhomogeneities in the refractive index of seawater (hereafter IRI).[4] The enhanced near-forward scattered energy can be explained simply by considering that the smallest scales of turbulence, the temperature inhomogeneities of scales of 1 mm, are responsible for light scattering. One of the main goals of this study is to verify this conjecture. The optical oceanography community has long acknowledged the effect of turbulence on light propagation in the ocean.[5–8] However, the importance of turbulence for optical measurements remains controversial. This controversy is in large part due to the required complexity of the instrument technology and its underwater use. Reliable experimental studies of the propagation of light in turbulent media are sparse,[9,10] partly because of the difficulty of making of angular measurements of scattered light in the presence of the unscattered light beam.

Even a numerical approach has been impeded because computers have been unable to accurately resolve details of turbulent flow with passive scalars such as temperature in the ocean where smaller scales than the velocity scales must be addressed. It is now possible to carry out numerical simulations, although they require hours of computation time on a supercomputer.[11] By contrast, the role of particles in the propagation of light in the ocean has received much attention. This is partly because phytoplankton, especially in the open ocean, are largely respon-

D. J. Bogucki and J. A. Domaradzki are with the Department of Aerospace Engineering, University of Southern California, Los Angeles, California 90089-1191. D. Stramski is with the Marine Physical Laboratory, Scripps Institution of Oceanography, La Jolla, California 92093-0238. R. Zaneveld is with the College of Oceanic and Atmospheric Sciences, Oregon State University, Corvallis, Oregon 97331.

sible for the variability in the scattering and absorption properties.[12,13]

The aim of this research is to compare the properties of the near-forward scattering on suspended particles and refractive-index inhomogeneities associated with temperature field under typical oceanic conditions. We first review the near-forward scattering on particles, then address sources of the inhomogeneities in the refractive index of seawater and calculate associated scattering on turbulence, and then we compare these results with particulate scattering. We also demonstrate the effects of near-forward scattering on particles and turbulence through laboratory experiment.

2. Modeling of Light Scattering by Particles

Before embarking on a discussion of our approach to model light scattering by marine particles, we first define the volume-scattering function (VSF), the major optical property that we use in this paper. The VSF describes the angular distribution of scattered radiation as the scattered radiant intensity $dI(\alpha)$ in a direction α per unit scattering volume dV divided by the incident irradiance E_0[14]:

$$\beta(\alpha) = \frac{dI(\alpha)}{E_0 dV}. \tag{1}$$

The associated total scattering coefficient b describes how much light has been scattered in all directions from the incident plane wave beam; it is defined as

$$b = 2\pi \int_0^\pi \beta(\alpha)\sin(\alpha)d\alpha. \tag{2}$$

The VSF and b are considered inherent optical properties. Following Preisendorfer,[15] these are properties whose magnitudes depend only on the substances present in the water and are independent of the geometric structure of the various light fields that may pervade it. The superposition principle applies to all inherent optical properties, and in the case of the VSF it implies that, if several substances are present in the medium, the global VSF results from the sum of the contributions from all constituents (as long as the single-scattering assumption is fulfilled). This allows us to calculate a total VSF in the case when the particulate ensemble is made up of particles of various size categories. In general, scattering by spherical particles can be calculated exactly from Mie theory.[16] The parameters in this theory are the refractive index and particle diameter scaled by light wavelength.

Our purpose now is to obtain reasonable estimates of the magnitude of the VSF in the near-forward directions associated with typical assemblages of marine particles by use of Mie-scattering calculations. We restricted these calculations to a single-light wavelength of 550 nm. This assumption is sufficient for our purposes because such calculations provide us with an approximate magnitude of the VSF that can be expected to occur over the entire visible spectral region.

The starting point for the Mie calculations is the generation of a hypothetical size distribution of marine particles and the selection of the value of the refractive index of particles. For the refractive index we assumed that particles are nonabsorbing, thus the imaginary part of the refractive index is zero. This is because absorption has a comparatively small effect on near-forward scattering, and most marine particles exhibit weak absorption in the green spectral region.[17] The addition of absorption would reduce the magnitude of the VSF, and we are not interested in obtaining conservative estimates of particulate VSF. On the contrary, for the purposes of comparison with turbulence-induced scattering, we are interested in estimates of near-forward particulate VSF that represent approximately the upper-limit values for typical assemblages of marine particles or even slight overestimates of this limit. The real part of the refractive index of marine particles can cover a fairly broad range, with living microorganisms typically characterized by a low index and the mineral particles by a high index.[17] We therefore made calculations for two hypothetical assemblages of particles: one with a low value for the real part of the refractive index of 1.04 (relative to seawater) and the other with a high index of 1.18. However, the scattering at very small angles, not larger than O(1°), depends only on the size of particle because it is nearly equivalent to diffraction by apertures of identical diameter.[18] Therefore the choice of refractive index is not critical for our present purpose of calculating the particulate VSF at very small angles.

To construct the particle size distribution (PSD) we used some major features from measurements of oceanic particles. Numerous particle size measurements with a Coulter counter showed that, for particle diameters D greater than approximately 1 μm, the distribution can be approximated by a power function with a slope being a negative number.[19,20] It was also found that the segmented description is often required to obtain the best fit to the Coulter counter data over the broad range of particle diameters extending to several tens of micrometers or so. Typically, the slopes are steeper for larger particles and less steep in the small size range. However, if a single value of the slope were to be chosen as the most typical one for the differential PSD, it would be −4. We therefore assumed such a value for the PSD used in our Mie calculations. Because large particles are known to have significant contribution to near-forward light scattering, we assumed that our PSD covers the diameter range as high as 1000 μm. The lower size cutoff was taken as 0.05 μm.

In addition to the slope, the power-law description of the PSD involves a second parameter that is related to the concentration of particles. Based on data collected on the Bahama Banks by Gordon,[19] we assumed that the cumulative concentration of particles greater than 1 μm in diameter is 7×10^{10} m^{-3}.
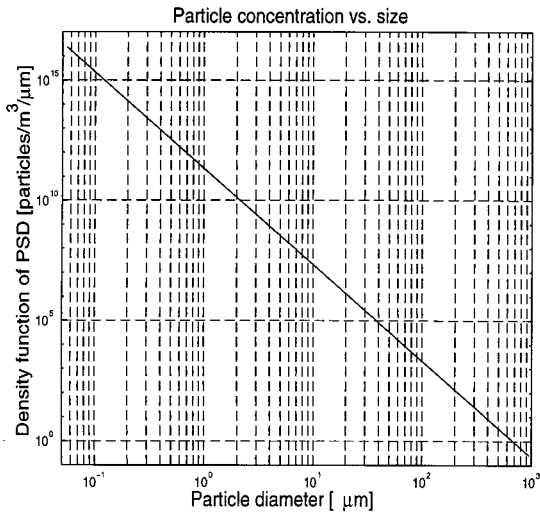
Fig. 1. Differential size distribution of oceanic particles used in our Mie-scattering calculations.
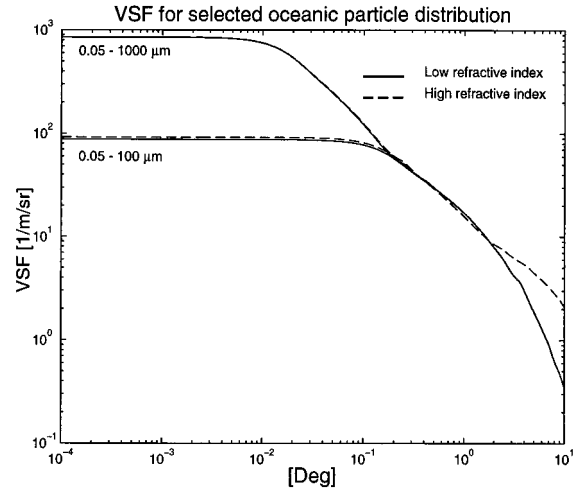

Fig. 2. Results of Mie-scattering calculations of near-forward VSF for the particle size distribution shown in Fig. 1. The VSF representing two upper size limits and two refractive indices are included.

Accordingly, the cumulative form of our PSD is $N = 7 \times 10^{10} \, D^{-3}$ particles $\times$ m^{-3} and the differential form is $dN/dD = 2.1 \times 10^{11} \, D^{-4}$ particles $\times$ m^{-3} μm^{-1} (Fig. 1). We note that this PSD represents a fairly high concentration of particles in seawater. Typical cumulative concentrations of particles with $D \geq 1$ μm in the upper layers of the Sargasso Sea is 4- to 20-fold less than the values assumed above.[19] In more turbid Baltic waters, the average value for such concentration estimated from size distributions measured by Jonasz[21] is approximately 4.5×10^{10} particles $\times$ m^{-3} with the standard deviation being as high as the average concentration.

To obtain the VSF representing our hypothetical PSD, we first divided the size distribution into 41 size classes and calculated the VSF associated with each size class separately. The Mie-scattering code was taken from Bohren and Huffman,[16] and the midpoint diameters of the size classes were used as input in these calculations. The resultant VSF was obtained as the sum of contributions from all size classes. As already mentioned, the calculations were made for $\lambda = 550$ nm for particles with low refractive index and high refractive index. The results for scattering angles as high as 10° are presented in Fig. 2. As can be seen, the particulate VSF exhibits the typical properties as experimentally obtained by Spinrad et al.,[2] namely the flat plateau for angles smaller than 10^{-2} to 10^{-1} deg and a decrease at larger angles. The magnitude of the VSF in the plateau is approximately 850 sr^{-1} m^{-1} for the entire particle population (D from 0.05 to 1000 μm). Note that the major contribution to this magnitude, approximately 90%, comes from large particles in the size range 100–1000 μm. Had we used the upper size cutoff of 100 μm instead of 1000 μm in our PSD, the estimated VSF values would have been approximately 10 times lower. We also note that the VSF curves for low-index and high-index particles are practically indistinguishable from each other for very small angles in the plateau region.

We can see that the refractive index begins to have an effect on the VSF for angles only greater than 1°.

Because the effect of refractive index is important for larger scattering angles, it is reflected in the values of the total scattering coefficient b. For our hypothetical assemblage of low-index particles, the calculated value of b is 0.24 m^{-1}, and for the assemblage of high-index particles $b = 1.079$ m^{-1}. (Note that under our assumption of no absorption, the scattering coefficient is equivalent to the beam attenuation coefficient.) Unlike the VSF at very small angles, the total scattering coefficient is almost entirely due to particles ≤ 100 μm; the contribution made by particles with D between 100 and 1000 μm is only 0.3 to 1.5% for high-index and low-index assemblages, respectively.

Our estimates of the near-forward VSF are expected to be close to the upper limit of the typical range for oceanic particles. This expectation is further justified by the fact that our PSD includes a comparatively high proportion of large-sized particles because, in reality, the slopes of size distribution may be steeper than -4 for large particles. However, it is also true that in very turbid coastal waters the particle concentrations, and the corresponding VSF, may still be higher than those described above.

3. Modeling of Light Scattering on Turbulence

A. Inhomogeneities in the Refractive Index

The real part of the refractive index of seawater varies with changes of temperature, salinity, and pressure; changes in the imaginary part of the refractive index of water are negligibly small compared with those of the real part.[22] The effect of pressure can be neglected for spatial scales of the order of a meter or smaller. The variance of the IRI (assuming that salinity and temperature fields are not correlated) can be expressed as the sum of the variance associated

with temperature and salinity: $\overline{(n^2)}^{1/2} = \overline{(n_T{}^2)}^{1/2} + \overline{(n_S{}^2)}^{1/2}$, where $\overline{()}$ denotes spatial averaging, n is the refractive index, and n_T and n_S are the contributions of temperature and salinity, respectively. For example, analysis of data from the Oregon coastal region shows that variance of the refractive index that is due to temperature is much larger than that due to salinity.[23] Consequently, only temperature-induced IRI are considered in this study and hereafter $n = n_T$. However, the results from this research are general and can be easily rescaled to the salinity-dominated regime of IRI.

B. Basic Equations

Turbulent inhomogeneities in the ocean are a source of light scattering. In general, full Maxwell equations describe the propagation of light in a turbulent medium. However, the time scale of light propagation is much less than the time scale of turbulence, and the light wavelength λ is much less than the length scale η of the smallest turbulent inhomogeneities, $\lambda \ll \eta$. In such situations the magnetic permeability of water and the effect of depolarization are negligible whereas the dielectric constant (refractive index) is assumed to be time independent. These assumptions allow one to reduce the full Maxwell equations to a scalar equation (Helmholtz equation):

$$(\nabla^2 + \kappa^2)E = -2\kappa^2 n(\mathbf{r})E, \qquad (3)$$

where E is any of the Cartesian components of the electric-field vector $\mathbf{E}$, κ is the light wave number, $\kappa = 2\pi/\lambda$, and $n(\mathbf{r})$ is the deviation of the local refractive index from its mean value. A transformation

$$E(x, y, z) = \psi(x, y, z)\exp(i\kappa z) \qquad (4)$$

and the assumption $\lambda \ll \eta$ allow one to simplify Eq. (3) to the parabolic (diffusionlike) Helmholtz equation[24]:

$$2i\kappa \frac{\partial \psi}{\partial z} + \nabla_T{}^2 \psi + 2\kappa^2 n\psi = 0, \qquad (5)$$

where the complex function ψ represents the phase and amplitude of light propagating in the z direction and $\nabla_T{}^2$ is the transverse Laplacian operator $\nabla_T{}^2 = \partial^2/\partial x + \partial^2/\partial y$.

Several approximation techniques have been developed for this equation.[25] We solved this equation numerically without any approximations and with the geometrical-optics approximation.[26] The latter approximation simplifies Eq. (5) if we are interested in propagation over short distances. If the distance of propagation L (in our calculations 0.25 m) obeys inequality $(L\lambda)^{1/2} \ll \eta$, where η is the scale of smallest temperature structure of the flow [typically of O(mm)], and diffraction effects are neglected, the

transverse Laplacian operator can be omitted and Eq. (5) can be solved analytically[24]:

$$\psi(x, y, z) = A_0(\mathbf{p})\exp\left[i\kappa \int_0^z n(x, y, z')\mathrm{d}z'\right], \quad z \le L, \qquad (6)$$

where A_0 is the initial value of $\psi(x, y, z = 0)$ at $z = 0$ and $\mathbf{p} = (x, y)$. This solution constitutes the first-order geometrical-optics approximation.[24] Because the second derivatives are neglected in this approximation, only changes in phase can be calculated.

The surface of the constant phase is given by

$$\Gamma(\mathbf{p}) = \int_0^L n(x, y, z)\mathrm{d}z \qquad (7)$$

at the distance $z = L$. The vector normal to $\Gamma(\mathbf{p})$ is

$$\mathbf{N} = \left[\frac{\partial \Gamma}{\partial x}, \quad \frac{\partial \Gamma}{\partial y}, \quad 1\right] \qquad (8)$$

and is parallel to the scattered ray direction.

The geometrical-optics approximation [Eq. (6)] used in this research was validated for the investigated range of distances and turbulent flows by use of the numerical solutions of the full Eq. (5).[26]

The light phase can be obtained with Eqs. (6) and (7) if the spatial distribution of the refractive index inside the investigated volume is known. Because there is a simple relation between temperature and refractive index,[27] the accurate spatial distribution of the temperature field in the turbulent medium is required.

Most geophysical flows usually have a large range of scales that depend on the Reynolds number of the flow. For example, an oceanic eddy presents temperature variability on scales ranging from O(10 m) to 1 mm. The relative contribution from different scales of the flow to the light scattering depends on the temperature variance spectrum (in the Fourier sense) $E_\theta(k)$ (three-dimensional spectrum of temperature fluctuations), where k is the wave number. The physical interpretation of $E_\theta(k)$ is that temperature variance for scales between k and $k + \mathrm{d}k$ is proportional to $E_\theta \mathrm{d}k$. In general the spectrum $E_\theta(k)$ depends parametrically on molecular properties, the kinematic viscosity v, and diffusivity D, as well as on the kinetic energy dissipation rate ϵ and the temperature variance dissipation rate χ. Both ϵ and χ can be measured in the ocean.[28] The rate of dissipation of turbulent kinetic energy ϵ determines the size of the smallest temperature structures through the Batchelor length scale $\eta_B = (vD^2/\epsilon)$.[4] From an optical perspective $\chi(\chi \propto \int_0^\infty E_\theta k^2 \mathrm{d}k)$ has the following interpretation: Larger values correspond to stronger temperature gradients across the smallest temperature structure of the flow. This situation is pictorially represented in Fig. 3. Therefore, for fixed molecular properties, the optical properties of a turbulent homogeneous and isotropic flow are characterized by two parameters: χ, which expresses the
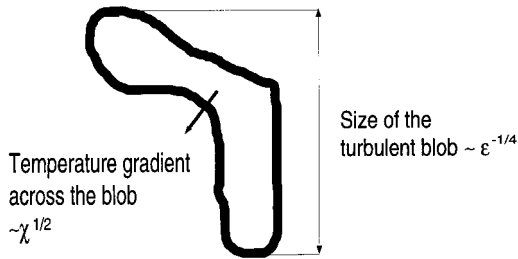
Fig. 3. Optical interpretation of the turbulent parameters χ and ϵ.

strength of the temperature gradient, and ϵ, which is inversely proportional to the size of the smallest flow structures. Typically, χ ranges from 10^{-2} °C^2/s a few meters below the surface[29] to 10^{-10} °C^2/s in the midwater column.[30] For ϵ the range is from 10^{-4} m^2/s^3 in a fairly energetic upper layer to 10^{-10} m^2/s^3 in the midwater column.[31]

Typical values and the vertical distribution of χ and ϵ for the midpart of the water column is shown in Fig. 4. The observed values of χ versus ϵ are not well correlated. This is shown on the scatterplot of χ versus ϵ in Fig. 5 for this vertical profile.

From the geometry of the problem (Fig. 6) and within the geometrical-optics approximation, the scattering angle α is

$$\tan(\alpha) = (\alpha_x^2 + \alpha_y^2)^{1/2}, \qquad (9)$$

where

$$\alpha_x = \frac{\partial \Gamma(\mathbf{p})}{\partial x}; \quad \alpha_y = \frac{\partial \Gamma(\mathbf{p})}{\partial y}. \qquad (10)$$

In the limit of small angles of near-forward angle scattering,

$$\alpha^2 \simeq (\alpha_x^2 + \alpha_y^2). \qquad (11)$$
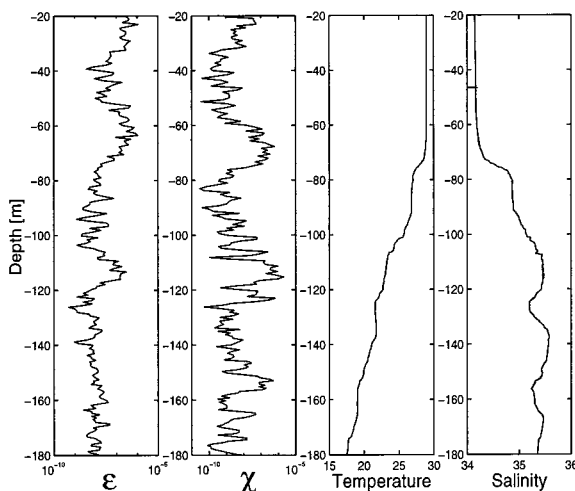

Fig. 4. Profiles of ϵ, χ, temperature, and salinity from the Oregon coast (courtesy of J. Moum[23]).
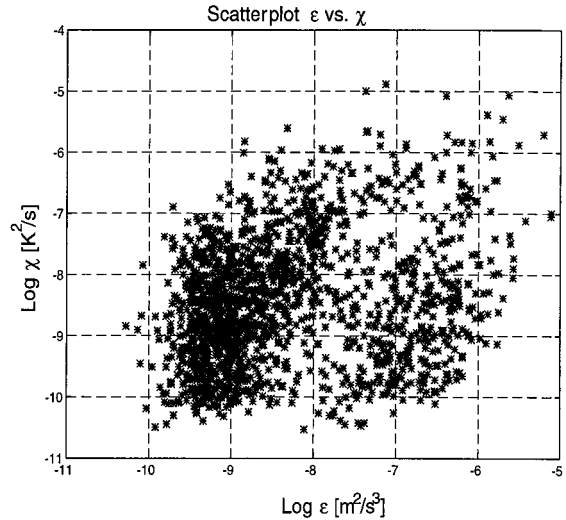

Fig. 5. Scatterplot of the observed ϵ versus χ in the data set from Fig. 4 (courtesy of J. Moum[23]).

Average value $\langle \alpha_x^2 \rangle$ is

$$\langle \alpha_x^2 \rangle = \lim_{\Delta x \to 0} \frac{\langle [\Gamma(\mathbf{p}_1) - \Gamma(\mathbf{p}_2)]^2 \rangle}{\Delta x^2}. \qquad (12)$$

Rytov et al.[32] show that, for isotropic fields,

$$\langle [\Gamma(\mathbf{p}_1) - \Gamma(\mathbf{p}_2)]^2 \rangle \propto L \int_0^\infty \Phi_{nn}(k)[1 - J_0(kp)]\mathrm{d}k, \qquad (13)$$

where $\Phi_{nn}(k)$ is the spectrum of the index of refraction n proportional to $E_\theta(k)/(4\pi k^2)$, $p = |\mathbf{p}_1 - \mathbf{p}_2|$, and J_0 is the Bessel function.
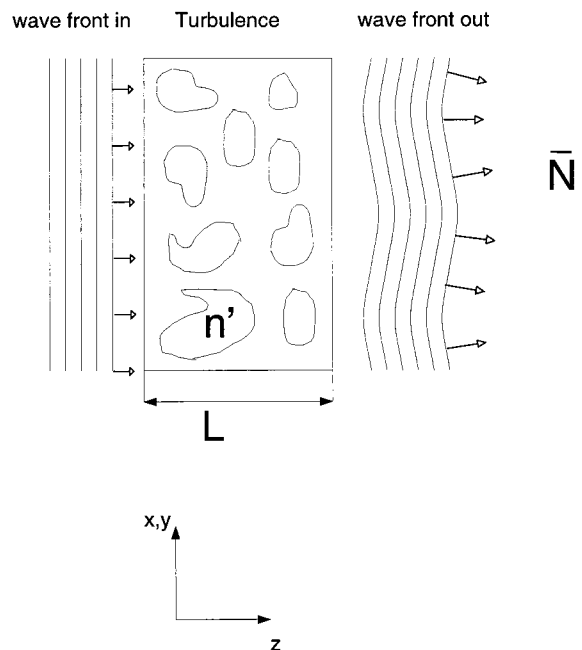

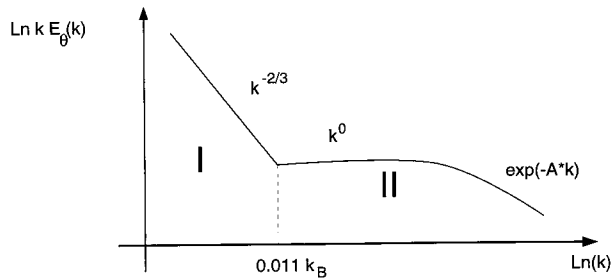Fig. 6. Schematic diagram underlying calculations of turbulence-induced light scattering.

Fig. 7. Value of $kE_\theta(k)$ for different scales of the flow. The physical scale is inversely proportional to k. Area I roughly marks the contribution to the scattering from the large-scale structures [less than 8% as calculated from Eq. (15)]. Area II denotes the contribution from the smallest, and most effective in scattering, scales.

The above formulas lead to the result for the mean variance of the scattering angle $\langle\alpha^2\rangle$:

$$\langle\alpha^2\rangle \propto L \int_0^\infty E_\theta(k)k\,\mathrm{d}k. \quad (14)$$

Because the function E_θ is always positive and so is k, the contributions from different scales to $\langle\alpha^2\rangle$ can be added to obtain the total variance of the mean scattering angle. Relation (14) implies that the variance of scattering angle for light propagated over distance L will depend most strongly on those scales for which the integrand $kE_\theta(k)$ is the largest.

Following Kolmogorov's local isotropy hypothesis, Obukhov[33] and Corrsin[34] predicted that scalar variance spectra at high Reynolds numbers (large scales) will have a $k^{-5/3}$ inertial subrange. The behavior of the variance spectra for larger wave numbers (smaller scales) depends on the Prandtl number $\mathrm{Pr} = \nu/D$. In oceanographic applications, temperature and salinity are important scalars and both have $\mathrm{Pr} > 1$. The case of $\mathrm{Pr} \gg 1$ was investigated theoretically by Kraichnan[35] who proposed the following scalar spectrum in the viscous-convective range[36]:

$$\frac{E_\theta(k\eta_B)}{\chi(\nu/\epsilon)^{1/2}\eta_B} = q(k\eta_B)^{-1}$$
$$\times [1 + (6q)^{1/2}k\eta_B]\exp[-(6q)^{1/2}k\eta_B], \quad (15)$$

where $\eta_B = 1/k_B$ is the Batchelor length scale and the universal constant q was found to be 5.26.[11] This is in agreement with results of Hill.[37]

By use of the standard value of the Corrsin–Obukhov constant, $C_{CO} = 0.5$, and the Prandtl number for temperature in water, $\mathrm{Pr} = 7$, the inertial range curve intersects the Kraichnan curve at $k\eta_B = 0.011$. To estimate relation (14) we use a composite model of the spectrum consisting of the inertial range curve for $k < 0.011k_B$, the Batchelor k^{-1} curve for $0.011k_B < k < k_B$, and the exponential falloff for $k > k_B$. The quantity $kE_\theta(k)$ is schematically represented in Fig. 7.

The integrated contribution of the large flow scales (marked on the figure as area I) to $\langle\alpha^2\rangle$ does not exceed 8% of that associated with small scales, i.e.,

scales smaller than $100\,\eta_B$. It means that, for the simplest homogeneous and isotropic turbulence, the light beam experiences the effects of broadening and steering mostly on the smallest details of the temperature field. This also implies that the results presented here for light scattering on homogeneous and isotropic flows are universal in a sense that they are independent of the large-scale details of the flow.

C.   Numerical Simulation of Light Scattering on Turbulent Flow

A spatial distribution of temperature in turbulent water was obtained by simulating numerically full Navier–Stokes equation with the passive scalar with Prandtl numbers of 3, 5, and 7.[11] The flow was assumed to be contained in a cube, and periodic boundary conditions in all three spatial directions were imposed on the independent variables. The domain was discretized in physical space by use of 240 uniformly spaced grid points in each Cartesian direction, resulting in the maximum resolution of 240^3 modes. The low wave-number modes for both velocity and temperature were forced. Calculations were carried out on the Cray C-90. It was demonstrated that all flows containing temperature as a passive scalar resulted in a universal self-similar distribution of the temperature variance field E_θ at small scales described well by the Kraichnan formula in Eq. (15). Thus the numerical simulations capture scales that, according to previous estimates, are responsible for light scattering on turbulence.

Our numerical experiment to propagate light through the simulated turbulent flow is as follows. First, as suggested in Ref. 11, we scale the strength of temperature fluctuations in the simulations $T(x, y, z)$ to prescribed values of χ and ϵ and then convert it into a spatial distribution of the refractive index $n(x, y, z)$. Subsequently we illuminate the computational volume with a plane-parallel wave by assigning a constant value to the function $\psi(x, y, z = 0)$. Because we illuminate our computational volume (240^3 size) with a plane-parallel wave, the phase and amplitude of the light is the same throughout the entrance plane. We then use Eq. (6) [or Eq. (5) for verification] to calculate the resultant $\psi(x, y)$ on the exit side of the computational volume. The value taken by the exponent of Eq. (6) at each (x, y) position describes how the initially plane-parallel wave front has been distorted by passage through the temperature inhomogeneities of the computational volume. This is illustrated schematically in Fig. 6.

Because the exit surface has 240^2 different pixel elements (of different $\mathbf{N}$), our resolution is limited to this number when determining the VSF. The final calculation of the VSF is done in a straightforward manner from Eq. (1). The calculated VSF for various possible χ and ϵ in the ocean are presented in Fig. 8. Here we note that the VSF for any given χ and ϵ can be approximated by a Gaussian function, determined by flow-dependent parameters:

$$\mathrm{VSF}(\epsilon, \chi, \alpha) = V_0(\epsilon, \chi)\exp\{-[\alpha/\alpha_0(\epsilon, \chi)]^2\}, \quad (16)$$
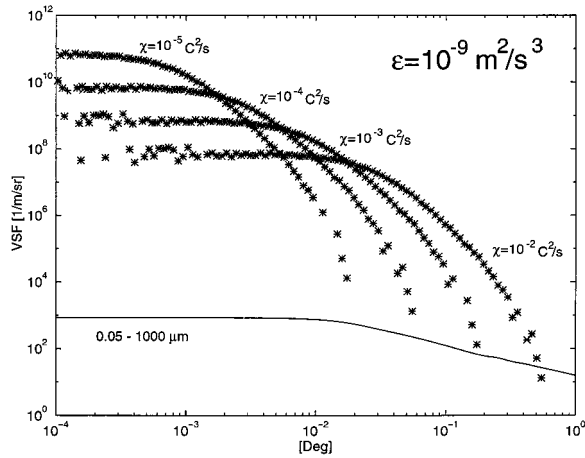
Fig. 8. Simulated VSF for a range of turbulent flows in the ocean, for varying χ and constant ϵ as indicated. The particulate VSF is shown for comparison (solid curve).

where V_0 describes the maximum value of VSF at $\alpha = 0$ and α_0 is the half-width.

The scattering angle standard deviation $(\langle \alpha^2 \rangle)^{1/2}$ is given in Table 1. The value of the scattering angle standard deviation depends on the propagation distance, so we use a constant optical path of 0.25 m. To obtain $(\langle \alpha^2 \rangle)^{1/2}$ for longer propagation distances L (within range L where $(L\lambda)^{1/2} \ll \eta$), the following formula [derived from relation (14)] can be used:

$$(\langle \alpha^2 \rangle)^{1/2}(L, \chi, \epsilon) = C_{0.25}(\chi, \epsilon)(L/L_0)^{1/2}, \qquad (17)$$

where L_0 in the case of our simulations is 0.25 m and $C_{0.25}(\chi, \epsilon)$ is the scattering angle deviation associated with this propagation distance. The values of V_0, α_0, and $C_{0.25}(\chi, \epsilon)$ were calculated for different flow conditions and are listed in Table 1.

4. Comparison of Volume-Scattering Function for Particles and Turbulence

The VSF corresponding to particles obtained earlier can be compared with the VSF corresponding to turbulence in the ocean. From Table 1 we can see that the turbulent flow scatters light most when χ is large and ϵ is low. Using the higher-limit values of χ, we estimated the VSF for a range of χ from 10^{-2} to 10^{-5} °C^2/s and for constant $\epsilon = 10^{-9}$ m^2/s^3, which is

Table 1. Volume-Scattering Function (V_0, α_0) and the Standard Deviation of the Scattering Angle $(\langle \alpha^2 \rangle)^{1/2}$

$\mathrm{Log}_{10}\,\epsilon$	$\mathrm{Log}_{10}\,\chi$	V_0	α_0 (deg)	$C_{0.25}(\chi, \epsilon)$ (rad)
-10	-2	2×10^3	1.1×10^{-1}	10^{-3}
-10	-4	2×10^5	1.1×10^{-2}	10^{-4}
-10	-6	2×10^7	1.1×10^{-3}	10^{-5}
-8	-2	2×10^5	5×10^{-2}	5×10^{-4}
-8	-4	2×10^7	5×10^{-3}	5×10^{-5}
-8	-6	2×10^9	5×10^{-4}	5×10^{-6}
-6	-2	2×10^6	1.1×10^{-2}	2.5×10^{-4}
-6	-4	2×10^8	1.1×10^{-3}	2.5×10^{-5}
-6	-6	2×10^{10}	1.1×10^{-4}	2.5×10^{-6}

likely to be encountered in the coastal region or in the open ocean (Fig. 8). For comparison, the particulate VSF is also plotted. It can be clearly seen that the turbulence-induced scattering dominates to angles as large as 0.1° for $\chi = 10^{-4}$ °C^2/s. We suggest that this is true regardless of particle concentrations because the magnitude of our particulate VSF is much lower. Because the VSF for turbulence scattering is very steep at small angles, it nearly guarantees that it will overcome particulate scattering at those very small angles even for much higher particle concentrations. Thus the dominant effect of the oceanic turbulence at very small angles seems to be a fairly universal fact.

The implications for underwater visibility applications are considerable as the scattering angle deviation $(\langle \alpha^2 \rangle)^{1/2}$ is as large as O(0.001 rad) (Table 1), implying that across a homogeneous turbulent layer of 10 m the smallest detail that can be resolved has, at best, dimensions of O(0.1 m). One has to keep in mind that those quantities are statistical averages, and they will differ in a given realization such that the mean of several realizations will be centered on the calculated values. The turbulent time scale corresponding to realistic dissipation values can be as short as O(0.1 s), implying that within that time the scattering angle fluctuates rapidly.

5. Laboratory Experiment

There have been previous attempts to measure the effect of light-scattering interaction with a convective turbulent flow.[10,38] These researchers usually recorded the statistics of the outgoing irradiance whereas the angular information of the scattered light could be only indirectly inferred. To compare our calculated VSF, we carried out a laboratory experiment at the University of Southern California Aerospace Fluid Dynamics laboratory where the source of turbulence was water in a convective cell. Turbulence for the experiment was generated by a heated element on the bottom and a cooling element on the top of the cell. The applied temperature gradient corresponded to a Rayleigh number of O(10^8), thus ensuring that the flow was fully turbulent. We used a 5-mW cw solid-state laser light ($\lambda = 640$ nm in vacuum) propagating through the cell. The path length was 0.1 m across the middepth of the tank. According to numerical simulations of such flows,[39] this ensures that light was propagating through a horizontally homogeneous, fully turbulent water volume. After traversing the turbulent volume, the light was projected on an opaque screen placed approximately 8 m away from the tank. The light intensity distribution was recorded on a tape by a camera attached to the VCR. The experiment was carried out for the estimated turbulence strengths of $\chi \approx 0.1$ and $\chi \approx 0.01$ °C^2/s with fairly constant $\epsilon \approx 10^{-6}$ m^2/s^3.

The recorded time series of spatial intensity distribution allowed us to estimate the scattering angle deviation $(\langle \alpha^2 \rangle)^{1/2}$ for various flows. The calculated (scaled to a 0.25-m path length) values were compa-
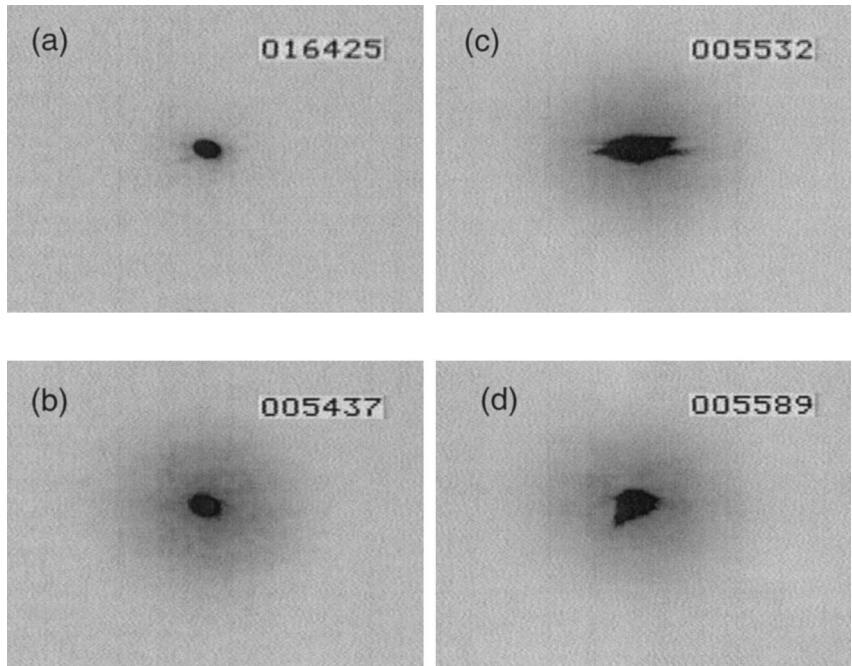
Fig. 9. (a) Light intensity distribution after propagation through water with no IRI and no beads. (b) Intensity distribution of scattered light by water with 10-μm beads. (c) and (d) Intensity distribution of scattered light by water with beads and turbulent IRI: two realizations a few seconds apart.

rable with simulated values given in Table 1, i.e., for $\chi \approx 0.1$, $(\langle \alpha^2 \rangle)^{1/2} \approx 10^{-3}$ rad, and for $\chi \approx 0.01$, $(\langle \alpha^2 \rangle)^{1/2} \approx 10^{-4}$ rad.

To visualize the differences between near-forward particulate and turbulent scattering, we performed additional experiments using a quasi-monodisperse assemblage of beads as particles (polystyrene beads of modal diameter 10 μm) and salt as a source of refractive-index inhomogeneities. We obtained the turbulent flow by rapidly stirring the water volume containing beads and salinity IRI. To optimize the visual effects we used unrealistically large concentrations of beads and salinity.

The light from the laser propagated through the cell with beads and IRI and was then projected on the opaque screen. The light intensity distribution was recorded with a camera system as in the previous experiment. The initial (no beads, no IRI) light distribution was also recorded. The results are shown in Fig. 9(a). The initial light distribution has a regularly shaped core of high-intensity light and weak-intensity background. In Fig. 9(b), representing beads with no turbulence, the distribution of light intensity scattered by beads was stationary in time, and the intensity decreased gradually away from the solid core of the primary beam. At some distance this intensity began to decrease more rapidly. This distance corresponds to the angle for which the rapid roll-off of the VSF begins (as confirmed by Mie calculations).

After introducing IRI, the situation changes drastically [Figs. 9(c) and 9(d)]. The solid core of the primary beam is replaced by irregularly shaped structures that change rapidly in time. This is consistent with the relation between the VSF for particulates and turbulence as shown in Fig. 8. This also illustrates that at small angles the VSF stops being

an inherent optical property because it is flow dependent. The light intensity distributions that is due to particles and turbulence have unique and different signatures, indicating that it might be possible to separate the two phenomena.

6. Conclusions

We have investigated numerically and experimentally the scattering of a light beam at small angles in a turbulent flow. We have found that the scales from the Batchelor k^{-1} range contribute most to the scattering process. We also compared the near-forward scattering by typical oceanic particulate assemblages with turbulence-induced scattering and found that turbulence dominates scattering for angles up to 0.1° over path lengths of the order of centimeters. Our results confirm that the frequently observed in situ high values of the VSF at small angles[1] are related to scattering on turbulent inhomogeneities in seawater. Furthermore, the initially homogeneous light becomes spatially inhomogeneous and highly intermittent after propagating through the turbulent region, giving rise to different signatures than those of particles. This turbulence-related intermittency will affect single realization measurements by increasing the variance of a scattering angle.

Reginald Hill for his detailed comments and helpful discussions. The comments and suggestions of an anonymous reviewer helped clarify an earlier version of this paper.

References

1. T. H. Petzold, "Volume scattering functions for selected ocean waters," Tech. Rep. SIO Ref. 72, (University of California, San Diego, 1972), pp. 1–79.
2. R. W. Spinrad, J. R. Zaneveld, and H. Pak, "Volume scattering function of suspended particulate matter at near-forward angles: a comparison of experimental and theoretical values," Appl. Opt. **17,** 1125–1135 (1978).
3. K. S. Shifrin, *Physical Optics of Ocean Water*, AIP Translation Series (American Institute of Physics, New York, 1988).
4. H. T. Yura, "Small-angle scattering of light by ocean water," Appl. Opt. **10,** 114–118 (1971).
5. W. H. Wells, "Theory of small-angle scattering," in *Electromagnetics of the Sea* (Advisory Group for Aerospace Research and Development, NATO, 92 Neuilly-Sur-Seine, France, 1973).
6. H. Hodara, "Experimental results of small-angle scattering," in *Electromagnetics of the Sea* (Advisory Group for Aerospace Research and Development, NATO, 92 Neuilly-Sur-Seine, France, 1973).
7. R. C. Honey and G. P. Sorensen, "Optical absorbtion and turbulence induced narrow-angle forward scatter in the sea," in *Electromagnetics of the Sea* (Advisory Group for Aerospace Research and Development, NATO, 92 Neuilly-Sur-Seine, France, 1970), pp. 39.1–39.7.
8. J. Zaneveld, R. Hodgson, and G. F. Beardsley, "Image degradation over sea water paths—a review," in *Electromagnetics of the Sea* (Advisory Group for Aerospace Research and Development, NATO, 92 Neuilly-Sur-Seine, France, 1973).
9. R. J. Hill, "Optical propagation in turbulent water," J. Opt. Soc. Am. **68,** 1067–1071 (1978).
10. R. A. Elliot, J. R. Kerr, and P. A. Pincus, "Optical propagation in laboratory-generated turbulence," Appl. Opt. **18,** 3315–3323 (1979).
11. D. Bogucki, A. Domaradzki, and P. K. Yeung, "Direct numerical simulations of passive scalars with $Pr > 1$ advected by turbulent flow," J. Fluid Mech. **343,** 111–130 (1997).
12. A. Morel and Y.-H. Ahn, "Optics of heterotrophic nanoflagellates and ciliates: a tentative assessment of their scattering role in oceanic waters compared to those of bacterial and algal cell," J. Mar. Res. **49,** 1–26 (1991).
13. D. Stramski and D. A. Kiefer, "Light scattering by microorganisms in the open ocean," Prog. Oceanogr. **28,** 343–383 (1991).
14. N. G. Jerlov, *Marine Optics* (Elsevier, New York, 1976).
15. R. W. Preisendorfer, *Hydrologic Optics*, Vol. 1 (National Oceanic and Atmosphere Administration, Washington, D.C., 1976).
16. C. F. Bohren and D. R. Huffman, *Absorption and Scattering of Light by Small Particles* (Wiley, New York, 1983), p. 530.
17. A. Morel and A. Bricaud, "Inherent properties of algal cells including picoplankton: theoretical and experimental results," in *Photosynthetic Picoplankton*, T. Platt and W. Li, eds., Can. J. Fisheries Aquatic Sci. **214,** 521–559 (1986).
18. J. B. Riley, "Laser diffraction particle sizing: sampling and inversion," Ph.D. dissertation (MIT–Woods Hole Joint Program in Ocean Engineering, Cambridge, Mass., 1987).
19. H. R. Gordon and O. B. Brown, "A theoretical model of light scattering by Sargasso Sea particulates," Limnol. Oceanogr. **17,** 826–832 (1972).
20. I. N. McCave, "Vertical flux of particles in the ocean," Deep-Sea Res. **22,** 491–502 (1975).
21. M. Jonasz, "Particle-size distributions in the Baltic," Tellus **35B,** 346–358 (1983).
22. M. Born and E. Wolf, *Principles of Optics* (Pergamon, Oxford, England, 1964).
23. J. Moum, College of Oceanic and Atmospheric Sciences, Oregon State University, Corvallis, Oreg. 37331 (personal communication, 1994).
24. V. I. Tatarski, *Wave Propagation in Turbulent Media* (McGraw-Hill, New York, 1961).
25. R. E. Hufnagel and N. R. Stanley, "Modulation transfer function associated with image transmission through turbulent media," J. Opt. Soc. Am. **54,** 52–61 (1964).
26. D. J. Bogucki, A. Domaradzki, R. Zaneveld, and T. Dickey, "Light scattering induced by turbulent flow," in *Ocean Optics XII*, J. S. Jaffe, ed., Proc. SPIE **2258,** 247–255 (1994).
27. M. J. Kennish, *Practical Handbook of Marine Sciences* (CRC Press, New York, 1989).
28. T. M. Dillon and D. R. Caldwell, "The Batchelor spectrum and dissipation in the upper ocean," J. Geophys. Res. **85,** 1910–1916 (1980).
29. D. M. Farmer and J. R. Gemmrich, "Measurements of temperature fluctuations in breaking surface waves," J. Phys. Oceanogr. **26,** 816–825 (1996).
30. T. M. Dillon, "The energetics of overturning structures: implications for the theory of fossil turbulence," J. Phys. Oceanogr. **14,** 541–549 (1984).
31. A. Anis and J. N. Moum, "Surface wave-turbulence interactions: scaling $\epsilon(z)$ near the sea surface," J. Phys. Oceanogr. **25,** 2025–2045 (1995).
32. S. M. Rytov, Y. A. Kravtsov, and V. I. Tatarski, *Principles of Statistical Radiophysics* (Springer-Verlag, Berlin, 1989).
33. A. M. Obukhov, "Structure of the temperature field in turbulent flows," Izv. Akad. Nauk SSSR Ser. Geogr. Geofiz. **13,** 58–69 (1949).
34. S. Corrsin, "On the spectrum of isotropic temperature fluctuations in isotropic turbulence," J. Appl. Phys. **22,** 452–469 (1951).
35. R. Kraichnan, "Small-scale structure of a scalar field convected by turbulence," Phys. Fluids **11,** 941–945 (1968).
36. R. C. Mjølsness, "Diffusion of a passive scalar at large Prandtl number according to the abridged Lagrangian interaction theory," Phys. Fluids **18,** 1393–1394 (1975).
37. R. J. Hill, "Models of the scalar spectrum for turbulent advection," J. Fluid Mech. **88,** 541–562 (1978).
38. A. S. Gurvich, M. A. Kallistrova, and F. E. Martvel, "An investigation of strong fluctuations of light intensity in a turbulent medium at a small wave parameter," Radiophys. Quantum Electron. **20,** 705–715 (1976).
39. J. A. Domaradzki, W. Liu, C. Hartel, and L. Kleiser, "Energy-transfer in numerically simulated wall-bounded turbulent flows," Phys. Fluids **6,** 1583–1599 (1994).